Combined rf and transport effects in magnetized capacitive discharges

M. D. Carter[a] and P. M. Ryan
Oak Ridge National Laboratory, Oak Ridge, Tennessee 37831-6169

D. Hoffman, W. S. Lee, and D. Buchberger
Applied Materials, San Jose, California 94086

V. Godyak
OSRAM Sylvania, Beverly, Massachusetts 01915

(Received 23 January 2006; accepted 12 July 2006; published online 12 October 2006)

Magnetic fields can be used to enhance the performance and operational envelope of rf capacitive discharges for semiconductor processing. Antennas in magnetized experimental fusion devices can experience similar rf processes that lead to surface erosion and degraded antenna performance. Two-dimensional modeling is needed to understand the combined effects of production and transport in these plasmas; however, magnetized plasma is a complicated medium because of tensor rf conductivity, anisotropic transport, and the fact that rf power alone sustains the plasma. In this paper, we give results from a model originally derived for studies of magnetized fusion and helicon discharges that has been adapted to capacitive discharges and compare the results with experimental data. The two-dimensional model combines the effects of the magnetic field on the plasma's rf properties and the bulk transport of plasma, including a sheath layer with finite thickness at the boundaries. A collisionless sheath model uses the rf fields in the sheath region, along with the density at the interface between the bulk plasma and the sheath, to determine the sheath thickness and to estimate the rectified dc potential. The driven rf fields are resolved inside the sheath region by including resistive dissipation caused by ion acceleration. These results are iterated with a model for transport of the bulk plasma to produce a global model of the sheath voltages and bulk rf plasma heating. The results at various iterative steps help isolate magnetic field effects that are caused by modification of the plasma's rf response from transport effects that are caused by the reduced electron mobility perpendicular to the magnetic field. The magnetic field can enhance confinement for some pressure regimes and magnetic configurations. More importantly, the magnetic field can restrict the motion of electrons that are heated by the rf, localizing the nonequilibrium distribution of electron energy and reducing the electron transport across magnetic field lines. Changes in the plasma rf response can also play a role in the behavior of the discharge by further localizing the rf power deposition in the plasma. © *2006 American Institute of Physics*. [DOI: 10.1063/1.2355436]

I. INTRODUCTION

Capacitive discharges are used in the semiconductor industry for a wide range of processes. The addition of static magnetic fields to these devices complicates their physics, but can significantly alter and improve their performance and operating range. Similar physics can be found near the rf antennas in magnetic fusion experiments where the rf can produce its own plasma, or excite existing plasma, that causes surface damage by ion acceleration and degradation of the rf performance.

In this paper, we consider frequencies that are more than ten times higher than the common industrial bias frequency of 13.56 MHz, and two-dimensional (2D) electromagnetic modeling is necessary. The goal of the work is to couple the results of the electromagnetic model to relatively simple models for the plasma transport and sheaths in order to identify important physical mechanisms and compare these effects with those found in experiments. The results of the model do not precisely simulate an actual device, but rather are intended to provide guidance concerning improvements that will be needed for future modeling efforts.

We isolate the dominant physical mechanisms from a combination of three basic types of effects in magnetized discharges. The first is the modification of the conducting properties of the plasma caused by magnetization of the electron motion on the rf time scale. These modifications are inherently two dimensional and the frequencies involved require an electromagnetic solution. The second type of effect is a change in the cross-field electron transport that directly modifies the quasineutral density distribution on a transport time scale. These transport effects can also modify the nonequilibrium electron energy distribution (EDF), reduce the transport of heated electrons across magnetic field lines, and lead to localization of the ionization source. The third type occurs inside the sheath layer where rf dissipation, rectification, and modification of the sheath capacitance can affect the rf circuit and plasma-surface interactions. Geometry further complicates these effects and their interaction with one another because the rf plasma properties are affected by both plasma density and magnetic field, while the plasma density is self-consistently produced by the deposited rf power.

[a]Electronic mail: cartermd@ornl.gov

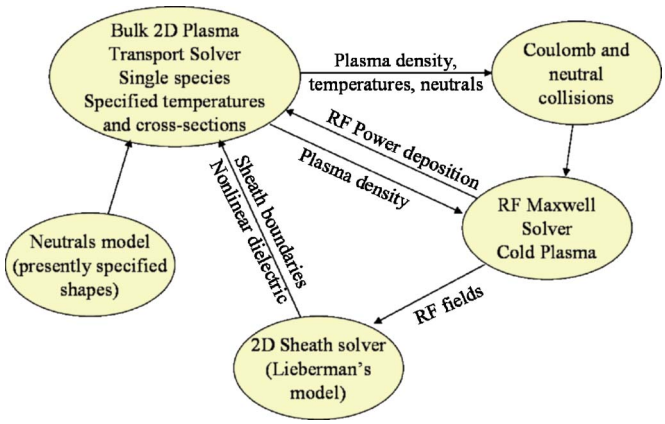

FIG. 1. (Color online) Models for bulk plasma transport, sheaths with finite thickness, and an electromagnetic model are iterated in the MORRFIC code to obtain solutions in magnetized rf generated discharges.

Many features of these devices and particularly the effects caused by the magnetization of the sheath layer have been studied by Kushner.[1] He[1] used a sophisticated model for the evolution of the plasma and neutral species, but considered only the radial component of the static magnetic field and an electrostatic rf model. In this paper, we adopt a complementary strategy, using relatively simple heuristic models for the plasma transport and sheaths, but retaining an electromagnetic model for the rf coupling suitable for high frequency applications in 2D static magnetic field geometries. We also study a system where the rf is applied to the plate opposite that of the wafer to be etched rather than to the wafer chuck as studied in Ref. 1. For the experimental and modeling results presented here, the axial static magnetic field component, rather than the radial component, is predominantly responsible for modifying the spatial uniformity of the discharge by inhibiting the transport of rf-heated electrons across magnetic field lines.

In a magnetized plasma, electromagnetic calculations require the plasma conductivity to be described as a full tensor in the quasineutral region rather than a scalar. These tensor formulations are not typically found in commercial electromagnetic solvers. Therefore, we have adapted codes developed for research on magnetized plasma systems[2] to address some of the issues that arise when curved magnetic fields are added to high frequency parallel plate capacitive reactors. Findings from this effort have proven useful for testing and improving these models. The algorithms are joined together iteratively, as shown in Fig. 1, and are collectively referred to as the modular oak ridge rf integration code (MORRFIC). Simplified assumptions are made for each of the individual models so that 2D results can be obtained for the iterative process without requiring excessive computation.

Following Fig. 1, the problem is initialized assuming a uniform distribution of rf power in the transport model to generate an initial guess for the plasma density. A collisionless rf sheath model, by Godyak[3] and Lieberman,[4] is used in the sheath layer, and the sheath is iterated with the transport model boundary that feeds the quasineutral bulk plasma into the sheath at the ion sound speed. Maxwell's equations are then solved in the frequency domain, with boundary conditions that are descriptive of the reactor geometry, using a linearized collisional cold plasma model in the quasineutral region and nonlinear resistivity (depending on the local electric field from the previous iteration) in the sheath. The resulting rf power and rf sheath fields are then used in the next iteration of the transport and sheath models.

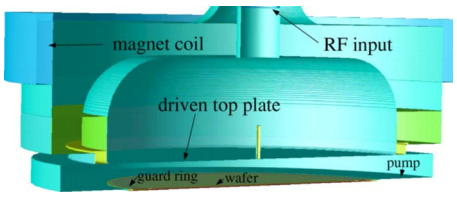

FIG. 2. (Color online) This cutaway shows the geometry of the modeled system in three dimensions. The top plate is driven by the rf and the bottom chuck is assumed to be held at virtual ground by other components in the rf circuit.

We drive the top plate of a magnetized capacitive discharge, as shown in Fig. 2, at frequencies greater than the electron cyclotron frequency. The precise frequency used for these reactors is proprietary information and may vary. For the simulations presented here, the model is driven at roughly 12 times the typical industrial value of 13.56 MHz. The gap between the driven top plate and the perfectly electrically conducting plane supporting the wafer is 0.032 m, and the wafer diameter is 0.3 m. The pump region shown in Fig. 2 is actually a three-dimensional structure with proprietary electrical isolation from the region that holds the wafer. These features are beyond the scope of the model presented here and allow the reactor to eliminate plasma production over the pump region. This effect is modeled by artificially terminating the plasma source in the model over the pump region and will be described in more detail when the model results are compared with experiment. We do not model any rf or dc bias applied to the grounded wafer. A cross-sectional cut in the r-z plane, taken from Fig. 2, is shown in Fig. 3 to more precisely define the system that is modeled. There is a single magnet coil outside and above the plasma production region. Precise details of this magnet system and the rf are proprietary information, and the model aspect ratio is further skewed relative to the actual device. Therefore, we specify the magnetic field in the model using an effective coil current for the experimental device. The reader should note that the magnetic field in the model causes the electron cyclotron frequency at the location of highest field in the discharge to approach the driven rf for a coil current of $\sim$20 A. All results presented here are for coil currents less than 20 A such that the driven frequency remains above the electron cyclotron frequency everywhere in the discharge.

The global modeling shows strong synergy between the rf coupling and the plasma source model as they are iterated to convergence for different applied magnetic fields. These effects are driven by changes in the plasma conductivity as well as changes in the electron energy and density distribution because of spatially localized power deposition and reduced electron transport across magnetic fields. We find that the radial etch rate profile can be significantly altered for magnetic fields that are low enough to leave the electron dynamics in the sheath reasonably unaffected.

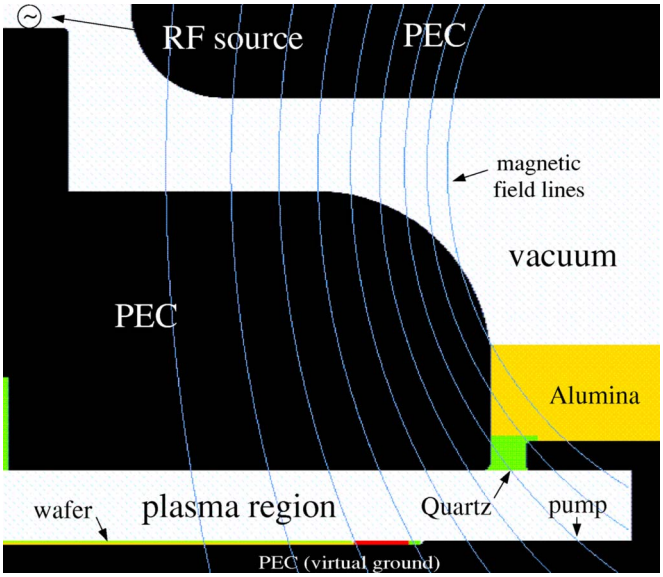

FIG. 3. (Color online) This schematic shows the radial and axial variations of the dielectric properties and magnetic field in a two-dimensional coaxial model. Perfect electrical conductors (PECs) are shown in black. Plasma is allowed to occupy the small region between the top conducting plate and the wafer.

The paper is organized as follows. The models for the physical processes in the MORRFIC simulation are described in Secs. II and III. Transport and ionization processes that determine the electron density distribution are discussed in Sec. II. The modeling of the plasma ionization source term, based on the rf power deposition, is described in Sec. II A. A discussion of the model for the ambipolar flux is given in Sec. II B. The solution of Maxwell's equations and the collisional cold plasma model for the quasineutral plasma are described in Sec. III. The technique for including the rf dissipation in Maxwell's equations caused by ion acceleration inside the sheath is described in Sec. III A. The sheath model, which is used for feedback of the sheath thickness and ion acceleration power to the other models, is described in Sec. III B. A simple etch rate model for comparison with the experimental data is described in Sec. III C.

In Sec. IV, we summarize the equations used in the MORRFIC simulation and present experimental results for comparison with the model for high power, low pressure conditions. These results show how the spatial redistribution of rf power heats electrons that are constrained in their motion perpendicular to the magnetic field. This heating determines the ionization reaction rate in the plasma source model. Localization of the heating, combined with reduced cross-field electron transport, is found to be the dominant effect in modifying the etch rate profile. In Sec. V, we compare results from the model with another set of experiments that tested the effects of radial and axial magnetic field components using two magnet coils symmetrically located above the wafer. The results show that the axial component of the magnetic field (normal to the wafer) plays the dominant role in modifying the etch profile rather than the radial component. The axial magnetic field reduces the scale length for electron energy relaxation perpendicular to the magnetic field lines. In Sec. VI, we summarize our results and describe future work that could improve the model.

II. MAGNETIC FIELD EFFECTS ON THE IONIZATION SOURCE AND TRANSPORT FLUX

The dimensions of the plasmas to be considered here are too small to justify a transport model that relies on thermal equilibration of the electrons. Thus, the standard closure methods for the fluid moments of the kinetic equations using Maxwellian energy distributions are suspect. The actual system is further complicated by the presence of both positive and negative ion species as well as many different neutral atomic and molecular states. For numerical simplicity, we begin with the continuity equation for the plasma inside the transport region assuming equal densities for electrons and singly charged positive ions,

$$\mathcal{S}(\mathbf{x}) = \nabla \cdot \Gamma_p(\mathbf{x}), \tag{1}$$

where $\mathcal{S}$ is the net volumetric source rate for electron-ion production, and Γ_p is the quasineutral particle flux.

Of chief interest is the ionization source, $\mathcal{S}(\mathbf{x})$, which depends on the electron energy distribution function (EDF), which in turn is controlled by the rf power deposition. Rather than attempting to model the EDF in detail, we adopt a phenomenological model of the ionization source, based on the rf power absorption per electron, to form an effective ionization rate coefficient, as described in Sec. II A. Relatively cold electrons can adjust to the ambipolar potential through processes that are crudely described by diffusion, but this ambipolar effect is considered separately from the transport of rf-heated electrons because the rf power deposition ultimately determines the ionization source. Our modeling shows that magnetic fields, coupled with spatially localized rf power deposition, can localize the ionization source to control the etch rate profile in the experiment.

As detailed in Sec. II B, a diffusive model of the unmagnetized ambipolar flux is not strictly valid,[5] but we use such a model anyway because it is numerically simple and it provides qualitatively correct behavior for the ambipolar plasma flux along magnetic field lines. The effect of classical cross-field diffusion is added heuristically to make a smooth transition from the unmagnetized to magnetized limits in a 2D diffusive model for the flux. The results of this modeling indicate that variations with magnetic field are not strongly dependent on the model for the ambipolar flux. However, they are sensitive to the parameters used in the ionization source calculation and hence the magnetically localized EDF.

A. Source rate model

For the systems discussed here, three-body volume recombination can be neglected, and we assume that all recombination occurs when plasma is driven into the surface. Because the rf alone sustains these plasmas, we assume that energetic electrons produce ionization at a rate proportional to the rf power absorbed per electron. To account for the redistribution of rf-heated electrons throughout the system, we average the rf power deposition over a region appropriate for relaxation of the electron energy distribution to derive the

local effective ionization rate, $\mathcal{S}(\mathbf{x})$, in Eq. (1). Thus, for unmagnetized plasma, the model assumes that electrons heated by the rf fields scatter their energy through the system to ionize gas over a range determined by their scale length for energy relaxation via electron-neutral collisions, λ_{rlx}. We define an effective cross section for inelastic electron-neutral collisions, σ_{rlx}, such that $\lambda_{rlx} \equiv 1/(n_n \sigma_{rlx})$. For process reactors it is reasonable to consider a uniform neutral density, although gas flow and localization of the heating can lead to significant variation in the excitation states of some neutral species.

For the devices considered here, λ_{rlx} is typically on the order of, or larger than, the dimensions of the device, so that rf power is fairly evenly redistributed by electron scattering throughout an unmagnetized system regardless of the spatial distribution of the rf damping. However, when a magnetic field is added, the redistribution of rf-heated electrons across magnetic field lines can be significantly inhibited, while the scattering of these electrons along magnetic field lines remains governed by λ_{rlx}. To account for this physics, the model averages the rf deposition profile over a flux tube having length along a magnetic field line of $\pm\lambda_{rlx}$, and a radius perpendicular to the field line equal to $\lambda_\perp = \min(\lambda_{rlx}, \rho_{\mathrm{EDF}}\sigma_{et}/\sigma_{rlx})$, where ρ_{EDF} is the gyroradius of an electron with energy representative of the ionizing population and σ_{et} is the total cross section for electron collisions with neutrals. The ratio, σ_{et}/σ_{rlx}, represents the number of collisional steps before a heated electron loses most of the energy gained from the rf in collision with neutrals. It is useful to separate the magnetic field effects from the energy effects by defining a quantity independent of the magnetic field that represents the energy of the rf-heated EDF, $E_{\mathrm{EDF}} \equiv m_e(\rho_{\mathrm{EDF}}\omega_{ce})^2$, where ω_{ce} is the electron gyrofrequency. For the work presented here, the bounds for the averaging process are truncated by rf sheath boundaries such that ionization inside the rf sheath layer is neglected.

Though not precise, this model for the source behaves in a physically reasonable manner by redistributing locally absorbed rf power over a region that is accessible by the rf-heated electrons as they move through the magnetic field and lose energy to the background neutral gas. For systems with λ_{rlx} and $\lambda_\perp$ everywhere greater than the system size, the model averages the rf power over the entire volume, giving a uniform source regardless of any spatial variation in the rf power deposition. For weakly collisional, but strongly magnetized electrons, the model yields a source proportional to an average of the rf power deposition along a magnetic field line. In a highly collisional regime where λ_{rlx} is everywhere less than the dimensions of the system, the local rf power deposition begins to directly determine the spatial distribution of the source term.

A power balance is needed to define an effective ionization reaction rate, $\langle \sigma_{\mathrm{ion}} v \rangle$, based on the absorbed rf power. Assuming most of the rf power is used to sustain energy losses caused by electron collisions with neutrals, we consider a phenomenological heat balance in steady state,

$$P_{\mathrm{rf}} - n_e \sum_n n_n \sum_j \langle \sigma_j v \rangle E_j \approx 0. \tag{2}$$

An average energy required for the creation of an electron-ion pair E_{ion} is then defined as

$$E_{\mathrm{ion}} \equiv \frac{\sum_n n_n \sum_j \langle \sigma_j v \rangle E_j}{\sum_n n_n \langle \sigma_i v \rangle}, \tag{3}$$

where σ_j is the cross section for inelastic collisions resulting in a loss of energy E_j in colliding with a neutral species of density n_n, σ_i is the cross section for ionization, and the $\langle\ \rangle$ indicate an average over the electron energy distribution. Thus, the power lost to radiation and ionization, $\Sigma_n n_e n_n \Sigma_j \langle \sigma_j v \rangle E_j$, is balanced by the absorbed rf power to create a source term for Eq. (1). The quantity, E_{ion}, can also be adjusted to account for other losses in the system, and is a free parameter in the model that is weakly dependent on details of the process as long as the supplied rf power is sufficient to reasonably sustain a discharge. In practice, E_{ion} can be determined empirically, and minimum values for ground-state neutrals are available from electron-beam experiments.[6]

In terms of an effective ionization rate, the source can be written as

$$S(\mathbf{x}) = \frac{\int_{V_i} P_{\mathrm{rf}} d^3x'}{\int_{V_i} E_{\mathrm{ion}}(\mathbf{x}') d^3x'} \equiv n_e n_n \langle \sigma_{\mathrm{ion}} v \rangle, \tag{4}$$

where V_i is a volume centered at $\mathbf{x}$ and extending over a region where heated electrons lose their energy as they scatter along their orbits. The effective reaction rate, $\langle \sigma_{\mathrm{ion}} v \rangle$, depends on the rf power delivered per electron inside the energy relaxation volume, V_i, which models the effect of a nonequilibrium, rf-driven, electron energy distribution function in the source term and/or the reduced ionization cost in heated regions where the population of excited neutral states is increased. For the work here, we assume E_{ion} is spatially uniform. Note that $S(\mathbf{x})$ in Eq. (4) depends only indirectly on n_e through P_{rf} so that the eigenvalue problem frequently solved in the literature for the continuity equation is replaced by the rf power deposition model and solved numerically in conjunction with Maxwell's equations.

B. Ambipolar flux model

Linear or nonlinear diffusive approximations can sometimes be used to simplify the form of Γ_p in single ion species plasmas, depending on the plasma parameters and the size of the device.[5,7,8] We follow Eq. (98) of Fruchtman *et al.*[5] to test the applicability of simplified models for Γ_p. The condition that must be satisfied for a linear diffusive model along magnetic field lines, or in an unmagnetized system, is

$$\frac{4}{b_P b_2^2} \ll 1, \tag{5}$$

where

$$b_P = L/2\lambda_{it},$$

$$b_2 = \frac{S\lambda_{it}}{n_e c_s} + \frac{4}{3}\sqrt{\frac{8T_g}{\pi T_e}}P(d),$$

$$P(d) = \frac{3\sqrt{\pi}}{8}d\left\{\left[\left(1+\frac{1}{d^2}-\frac{1}{4d^4}\right)\mathrm{erf}(d) + \frac{1}{\sqrt{\pi}}\left(\frac{1}{d}+\frac{1}{2d^3}\right)\exp(-d^2)\right]-1\right\},$$

where $d=v/\sqrt{2T_g/m_i}$, m_i is the ion mass, and λ_{it} is the mean free path between ion collisions with neutrals. The ion flow velocity, v, is bounded between zero somewhere inside the quasineutral region of the plasma and the ion sound speed, c_s, at the sheath boundary. A nonlinear diffusive model[7,8] can be used in the limit opposite that given by Eq. (5), while a fully nonlinear model is required when $4/(b_P b_2^2)\sim 1$.

For an argon plasma with parameters typical of the modeling results presented later, $T_g \approx 0.1$ eV, $T_e \approx 1.5$ eV, $L=0.03$ m, and $\lambda_{it}\approx 2\times 10^{-3}$ m, the Paschen parameter b_P is ≈ 7. However, effects caused by volume ionization and finite neutral gas temperature are also included in Eq. (5). For this device, we consider $\sim 0.15 < S\lambda_{it}/(n_e c_s) < \sim 0.30$, giving $\sim 0.5 < b2 < \sim 0.7$ and resulting in the range of conditions: $\sim 1 < 4/(b_P b_2^2) < \sim 3$. Thus, we must conclude that a fully nonlinear model is required to accurately model the ambipolar flux throughout the entire system, even in a simple argon plasma. The development of such a complete model for the transport requires effort well beyond the scope of this work, and requires further investigation of other effects concerning closure of the fluid equations, and the EDF. So we again resort to a qualitative heuristic model for the ambipolar plasma flux and connect the transport region to a distinct sheath layer using a boundary condition.

We wish to retain a 2D bulk plasma response, including the curved magnetic fields in the actual device, that can be adapted to handle collisional transport across magnetic field lines. The transport model must be computationally expedient and allow stable iteration with both the calculation of rf power deposition and a sheath layer of varying thickness around the perimeter of the plasma. Because of these constraints, and the fact that it provides a qualitative ambipolar description of the bulk plasma, we incrementally extend a diffusion model for Γ_p from previous work[2] to two dimensions, even though it is not strictly valid along magnetic field lines for the plasma parameters to be modeled. In this model, ambipolar diffusion controls the particle flux in all directions for cases where collisional processes prevent the charged particles from feeling the static magnetic field. The ambipolar potential also controls the particle flux along magnetic field lines if the electron motion perpendicular to the magnetic field is restricted.

For a plasma with a single species of singly charged ions, the ambipolar diffusion coefficient in a weakly ionized system of sufficient size is given by

$$D_A = \frac{C_s(1+T_i/T_e)}{n_n(\sigma_{et}\sqrt{m_e/m_i}+\sigma_{it}\sqrt{T_i/T_e})}, \tag{6}$$

where n_n is the neutral gas density, σ_{et} and σ_{it} are the total scattering cross sections with neutrals for electrons and ions, respectively ($\sigma_{et}\sim$ a few $\times 10^{-19}$ m^2, and $\sigma_{it}\gtrsim\sigma_{et}$, depending on the ion species), m_e is the electron mass, m_i is the ion mass, T_e is the electron temperature, T_i is the ion temperature, and $C_s\equiv\sqrt{kT_e/m_i}$ is the ion sound speed.

For the discharges considered here, the ion temperature is expected to be reasonably close to the temperature of the neutrals, roughly 1000 K $\approx$ 0.1 eV.[9] For electron temperatures around 1 eV, the ratio of T_i/T_e can be ignored compared with 1 in the numerator of Eq. (6). However, the electron-ion mass ratio, $m_e/m_i\approx 10^{-5}\ll T_i/T_e$ for Ar, so that T_i typically cannot be ignored in the denominator of Eq. (6). Frictional effects caused by the directed ion motion modify the ambipolar flow, and the ambipolar diffusion coefficient in the limit of negligible $\sqrt{m_e/m_i}$ is

$$D_A \approx C_s L_i, \tag{7}$$

where

$$L_i \equiv \frac{1}{n_n\sigma_{it}}\sqrt{\frac{T_e}{T_i}} \tag{8}$$

is the gradient scale length for the electrostatic potential.

The magnetic field can inhibit electron motion perpendicular to the magnetic field lines described by a cross-field diffusion coefficient, D_ρ. The magnetization of the plasma determines D_ρ, and for this application, we consider a classical cross-field diffusion coefficient of

$$D_\rho \approx \frac{n_n\sigma_{et}v_{te}}{2}\rho_e^2, \tag{9}$$

where v_{te} is the electron thermal speed, and ρ_e is the electron gyroradius.

Relatively cold electrons can adjust to the ambipolar potential through processes described by a diffusion coefficient, but this effect must be considered separately from the transport of heated electrons which affects the ionization source described in Sec. II A. The transport of bulk electrons across magnetic field lines is affected by the magnetic field strength when cross-field diffusion of electron gyro-orbits becomes smaller than the ambipolar diffusion, that is, when $D_A\gtrsim D_\rho$. In the simplified case of similar total collision cross sections for electrons and ions, $\sigma_{et}\approx\sigma_{it}=\sigma$, the magnetic field begins to affect classical diffusion when the typical collisional mean free path with neutrals, $\lambda\equiv 1/(n_n\sigma)$, becomes greater than $\sqrt{\rho_e\rho_i/2}$, where ρ_i is the ion gyroradius. In contrast, the redistribution of the 2D rf power deposition by the transport of heated electrons becomes constrained by the axial magnetic field when $\rho_{\mathrm{EDF}}\sigma_{et}/\sigma_{rlx}$ becomes smaller than the radial scale length for the device. For the weakly ionized argon plasmas considered here, $\sigma_{et}/\sigma_{rlx}\approx 50$.

In cases where the cross-field diffusion is greatly reduced by a strong magnetic field, ambipolar diffusion is used along magnetic field lines regardless of the magnetic field strength. Thus, a reasonable diffusive transport model that

accounts for both perpendicular and parallel diffusions in the system over a wide range of magnetic fields and pressures can be generated using

$$D_{\perp} \approx \frac{D_A D_{\rho}}{D_A + D_{\rho}} \tag{10}$$

and

$$D_{\parallel} \approx D_A, \tag{11}$$

where the subscripts $\parallel$ and $\perp$ denote coordinates parallel and perpendicular to the magnetic field lines, respectively. In a 2D diffusion approximation using an orthogonal coordinate system aligned parallel and perpendicular to the magnetic field lines,

$$\Gamma_p = -D_{\parallel}\frac{\partial n(\perp,s)}{\partial s} - D_{\perp}\frac{\partial n(\perp,s)}{\partial \perp}, \tag{12}$$

where s is a coordinate in the direction of $\mathbf{B}$. The operators in cylindrical coordinates are

$$\frac{\partial}{\partial s} \equiv b_r\frac{\partial}{\partial r} + b_z\frac{\partial}{\partial z} \tag{13}$$

and

$$\frac{\partial}{\partial \perp} \equiv b_z\frac{\partial}{\partial r} - b_r\frac{\partial}{\partial z}. \tag{14}$$

For the overall transport model, Eqs. (12)–(14) are used with a cylindrical divergence operator and Eq. (4) for the source to solve the continuity equation [Eq. (1)] numerically for n_e. The boundary conditions near solid surfaces are modeled by surrounding the surface with a 2D sheath layer. Plasma diffusion into the sheath region is handled as a boundary condition for Eq. (12),

$$\left[D_A\frac{\partial n}{\partial s}\right]_{s_1} = -[C_s]_{s_1}n_1, \quad \left[D_A\frac{\partial n}{\partial s}\right]_{s_2} = [C_s]_{s_1}n_2, \tag{15}$$

where s_1 and s_2 denote the locations along a magnetic field line where the quasineutral plasma meets the sheath region. The values, n_1 and n_2, are the plasma densities at s_1 and s_2, respectively.

III. SOLUTION OF MAXWELL'S EQUATIONS

For the electromagnetic fields, Maxwell's equations are solved in 2D with a local dielectric tensor (required for magnetized plasma),

$$\nabla \times \mathbf{E} = i\omega\mathbf{B}, \quad \nabla \times \mathbf{B} = \mu_0\mathbf{J}_{\text{ext}} - i\omega\epsilon_0\mu_0\tilde{K}\cdot\mathbf{E}, \tag{16}$$

where $\mathbf{E}$ and $\mathbf{B}$ are the complex electric and magnetic rf field vectors, respectively, with implicit $\exp(-i\omega t)$ time dependence, $\tilde{K}$ is the nine component local dielectric tensor, and $\mathbf{J}_{\text{ext}}$ represents rf current sources provided by an external generator or antenna. In the numerical solution, the rf magnetic fields are eliminated from Eq. (16) and the resulting $\nabla\times\nabla\times$ operator is conservatively differenced on a staggered mesh in cylindrical coordinates. All units are mks.

For regions where linear charged particle orbits are valid on the rf time scale (not in the sheath), the dielectric tensor in cold plasma can be written as[10]

$$\tilde{K_c} = \begin{pmatrix} S & -iD & 0 \\ iD & S & 0 \\ 0 & 0 & P \end{pmatrix}, \quad \mathbf{E} = (E_{\perp 1}, E_{\perp 2}, E_{\parallel}). \tag{17}$$

In the right-handed orthogonal coordinate system of Eq. (17), $\{\perp 1, \perp 2, \parallel\}$, the $\parallel$ direction is along the static magnetic field and $\perp 1$ is in the direction of perpendicular wave propagation. In a cylindrical $\{\hat{r},\hat{\theta},\hat{z}\}$ coordinate system with no azimuthal static magnetic field, such as those presented here, $\perp 2 = \hat{\theta}$, and $\tilde{K_c}$ is rotated into cylindrical coordinates. The quantities, S, D, and P, are described in the cold plasma limit as

$$S = S_c \equiv 1 - \sum_j \omega_{pj}^2/(\omega^2 - \omega_{cj}^2),$$

$$D = D_c \equiv \sum_j (\omega_{cj}/\omega)\omega_{pj}^2/(\omega^2 - \omega_{cj}^2),$$

$$P = P_c \equiv 1 - \sum_j (\omega_{pj}^2/\omega^2), \tag{18}$$

where $\omega_{cj} = q_j B_0/m_j$ is the cyclotron frequency of the jth species, $\omega_{pj} = \sqrt{q_j^2 n_j/(\epsilon_0 m_j)}$ is the plasma frequency for the jth species, B_0 is the static magnetic field strength, ϵ_0 is the permittivity of free space, and q_j, m_j, and n_j denote the charge (with sign), mass, and density of the jth species, respectively. Collisional damping based on the neutral collision frequencies is included in the cold plasma model by allowing the species mass to be complex and multiplying m_j by $(1 + i\nu_j/\omega)$, where ν_j is the effective total collision frequency for the jth species.

Solutions to Eq. (16) are obtained by assuming azimuthal symmetry for the plasma properties, Fourier analyzing the rf field components according to

$$\mathbf{E}(\mathbf{r},t) = \sum_{-\infty}^{\infty} \mathbf{E}_m(r,z)e^{i(m\phi-\omega t)}, \tag{19}$$

and numerically solving Maxwell's equations in the r-z plane, where r and z are the radial and axial coordinates, respectively. The numerical solution is obtained using finite difference techniques in cylindrical coordinates with a staggered Yee grid, typcially with a radial resolution of 0.6 mm and an axial resolution (across the sheath) of 0.08 mm. For this 2D system, the rf drive is also symmetric in the azimuthal direction, so the Fourier decomposition in Eq. (19) need only to consider $m=0$.

For the very high frequencies considered, the 2D electromagnetic solution requires a careful description of the grounding paths provided by the perfectly electrically conducting (PEC) components. The 2D electromagnetic solution is found in cylindrical geometry with PEC boundary conditions on the outer limits of the solution domain. Within the computational domain, additional PEC regions can be added to construct the driven (top) plate, the wafer bias grid, and

the conducting paths leading to the edge of the domain. Exposed corners are rounded to a prescribed radius of curvature to prevent localized peaking of the electric fields near corners. A specified rf current at the driving frequency is imposed across a small vacuum gap far from the region of interest, as shown in Figs. 2 and 3, to provide the only rf power source in the calculation. Energy conservation is used to check the convergence of the solution, and the integrated incoming power typically matches the absorbed power to within six decimal places.

Regions with scalar dissipative dielectric properties are specified where desired to model the other components of the chamber. The plasma tensor properties are described between the driven plates in the quasineutral plasma region using Eq. (17) and results from the transport model with the static magnetic field calculated using a filament model for the magnet coils. The nonlinear dissipation of the rf in the resistive sheath region is described below.

A. Nonlinear resistivity in the sheath

The resistive properties of the plasma sheath are nonlinear and are included in the solution to Maxwell's equations by explicit iteration. We follow a procedure similar to that of Jaeger *et al.*,[11] except that we retain the finite sheath thickness in the rf calculations. The ion acceleration through the sheath requires the system to supply an average power flux of

$$\Gamma_{\mathrm{nl}}^{E} = c_s n_s Z e V_0, \tag{20}$$

where c_s and n_s are the sound speed and density at the sheath/transport interface, Z is the ion charge state, e is the electron charge, and V_0 is the rectified dc voltage. This power is supplied directly to the ions by rectification of the driven rf fields in the sheath. We model the time-averaged power transfer to the sheath at the driven frequency by a uniform conductivity across the sheath layer,

$$\frac{1}{2}\mathrm{Re}\left[\int_0^{\Delta} \mathbf{E}\cdot\mathbf{J}_{\mathrm{nl}}^{*} ds\right] \equiv \sigma_{\mathrm{nl}}\langle E_n^2\rangle \Delta/2, \tag{21}$$

where s is the distance across the sheath in a direction normal to the surface, Δ is the sheath thickness, $\mathbf{J}_{\mathrm{nl}}$ is the nonlinear rf current at the driven rf, σ_{nl} is the effective nonlinear conductivity of the sheath, and $\langle E_n^2\rangle$ is the average of the square of the rf electric field component normal to the surface across the sheath layer, E_n.

Note that some care is required on the rf time scale to make the transition from a linear rf response in the quasineutral bulk plasma to the sheath layer because of the resonance in the linear plasma response at $\omega=\omega_{pe}$.[12] If the time-averaged electron density passes through a value such that $\omega=\omega_{pe}$ in Eq. (18), then care must be taken to ensure that the linear orbits used to calculate Eq. (18) remain valid. For the work here, we assume a sharp transition between the bulk plasma region where Eq. (18) is used and the nonlinear sheath region where nonlinear orbits occur on the rf time scale. Setting the right hand sides of Eqs. (20) and (21) equal gives

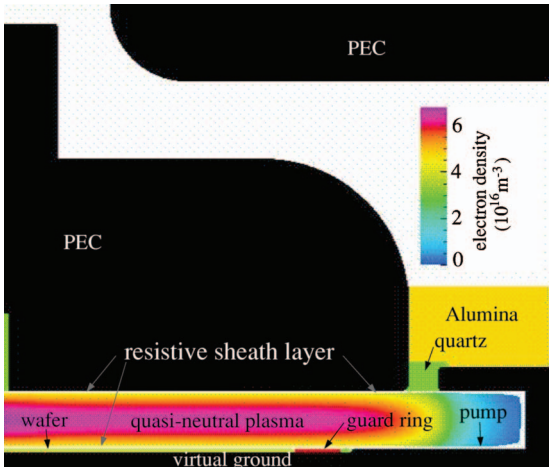

FIG. 4. (Color) The 2D sheath model tracks the sheath thickness in r and z coordinates, using the previous iterates to determine the self-consistent sheath thickness. The thickness is based on a collisionless model using local values of the dependent quantities. The bulk plasma density inside the sheaths is determined by the transport model with the source obtained from the rf power deposition in the rf model. The electrical circuit is assumed to provide a virtual ground at the wafer location. Note the short at the outer edge of the pumping port may affect results with relatively high magnetic fields.

$$\sigma_{\mathrm{nl}} = \frac{2c_s n_s Z e V_0}{\langle E_n^2\rangle \Delta} \tag{22}$$

inside the sheath region. With this formulation, a nonlinear sheath model can provide the relationships between Δ and V_0 given E_n from a previous solution to the rf model, and c_s and n_s from the transport model.

Transformation from the normal component coordinates back to the cylindrical coordinates of the 2D rf model gives the nonlinear conductivity tensor,

$$\tilde{\sigma}_{\mathrm{nl}} = \sigma_{\mathrm{nl}}\begin{pmatrix} n_r^2 & 0 & n_r n_z \\ 0 & 0 & 0 \\ n_r n_z & 0 & n_z^2 \end{pmatrix}, \tag{23}$$

where n_r and n_z are the cylindrical components of the surface normal vector.

We further assume that there is no modification of the real dielectric response caused by the time-averaged electron distribution inside the sheath. Thus, we take the real part of the dielectric in the sheath region to be one, giving a nonlinear dielectric for use in Eq. (16) inside the sheath,

$$\tilde{K}_{\mathrm{sheath}} = \tilde{I} + i\tilde{\sigma}_{\mathrm{nl}}/\omega\epsilon_0, \tag{24}$$

where $\tilde{I}$ is the identity tensor. Numerical diagnostics track the sheath characteristics in the system, as shown in Fig. 4, recording the various quantities in Eqs. (20)–(23) for use in following iterations. Upon convergence, the integrated power deposition in the sheath region from the solution to Eq. (16), using Eq. (24) in the sheath region, becomes equal to the nonlinear ion heat flux to the surface.

Stochastic heating may also occur at the oscillating interface between the sheath and the bulk plasma. We crudely model this effect by adding a uniform effective collision frequency ν_F to the electron-neutral collision term[13] in Eq. (18).

This effective collision frequency is enhanced because of the high frequency and relatively low pressure in this device.[14,15] We use a uniform value of $\nu_F = 4 \times 10^8\ \mathrm{s}^{-1}$ to simulate stochastic heating in all of the work presented here, but note that the results are somewhat sensitive to the value of ν_F. An improved model for this effect requires a computational effort beyond the scope of this work.

B. Sheath model

Following the notation of Lieberman,[4] the nonlinear dynamics is described by a harmonic expansion of the voltage across the sheath,

$$V(t) = \sum_{k=0}^{\infty} V_k \cos(k\omega t). \tag{25}$$

In Eq. (25), V_0 denotes the rectified dc voltage across the sheath, V_1 denotes the rf voltage amplitude driven across the sheath by the rf transmitter, and $V_{k>1}$ denotes harmonic voltage amplitudes. Given the driven rf voltage, V_1, the sheath model can be used to determine the dc voltage, V_0, the sheath thickness, the electron density profile throughout the sheath, and all the harmonic voltages.

Assuming V_1, T_e, and n_s are known, a collisionless sheath thickness is given by

$$\Delta = \lambda_e (\pi H)^{1/2} (2 + 5\pi H/12) + \Delta_0, \tag{26}$$

where $\lambda_e = 7430\sqrt{T_e/n_s}$ is the Debye length at the bulk-sheath interface,

$$H = \frac{[1 + (2V_1 C)/(\pi T_e)]^{1/2} - 1}{C}, \quad C = \frac{5\pi}{6} - \frac{1024}{675\pi}, \tag{27}$$

and Δ_0 is a limiting value for the sheath thickness when the rf electric field becomes small.[16] It is important to use a value of Δ_0 that is at least several λ_e in order to prevent a numerical collapse of the sheath during the iteration process and its subsequent shorting by either direct plasma currents or displacement currents. A value of $\Delta_0 = 10\lambda_e$ was used for simplicity in this work, although a more complete model for Δ_0 is available.[16]

To calculate the rectified dc voltage, V_0, information from both sheaths in the circuit is needed. Magnetic field connections, 2D effects, and imbalances in the rf voltage at opposite connected sheaths greatly complicate the details of the dc potential. Also, for magnetic fields such that $\rho_e < \Delta$ and $\omega_{\mathrm{rf}} < \omega_{ce}$, the electron motion through the sheath can be affected, invalidating the assumptions used to derive Eq. (26). These complications are beyond the scope of the present work. However, we proceed heuristically using

$$V_0 = \frac{\pi H T_e}{4}\left(3 + \frac{9\pi H}{8}\right) \tag{28}$$

for each sheath, and we later average the V_0 values obtained at opposite plates. Thus, while the model remains reasonable for field lines that are normal to the solid surface, it is not valid if the field lines become nearly tangential to the surface for $\omega_{\mathrm{rf}} < \omega_{ce}$. Thus, for the results in this paper, we consider only $\omega_{\mathrm{rf}} > \omega_{ce}$ (coil currents ¡20 A).

C. Etch rate model

Etch rate estimates are needed from the model to compare with etch rate measurements from the experiments. The actual etch rate is strongly influenced by the wafer bias and the halogen content of the plasma, which is proprietary information. However, experimental conditions were chosen to reduce these effects and allow reasonable comparison with the argon model. To provide a diagnostic with relevance to an experimentally measurable quantity, we calculate the etch rates for physical etching of argon on polysilicon using the formula[17]

$$\epsilon = 0.0375(\sqrt{\langle V_0 \rangle} - \sqrt{E_{\mathrm{th}}})\Gamma_p \tag{29}$$

with ϵ in units of Si at. $\mathrm{m}^{-2}\ \mathrm{s}^{-1}$, where Γ_p is the particle flux to the wafer, and a value of $E_{\mathrm{th}} = 16$ V was used. The values of the rf voltage were converted to dc voltages using Eq. (28) and the two values at each radius location were averaged to obtain $\langle V_0 \rangle$ in Eq. (29). The actual particle flux at the plasma-sheath interface over the wafer, Γ_p, was obtained from the transport model.

IV. COMPARING THE MODEL TO THE EXPERIMENT

For the MORRFIC simulation here, the 2D transport module numerically solves the continuity equation, Eq. (1), inside the bulk plasma region using Eq. (4) for the ionization source, $\mathcal{S}$, and Eqs. (10)–(14) to model the ambipolar particle flux, Γ_p, with the boundary condition at the interface with the sheath region given by Eq. (15). The 2D [$m=0$ in Eq. (19)] electromagnetic module for the rf fields solves Eq. (16) with the dielectric tensor, $\tilde{K}$, given by the cold plasma result, $\tilde{K}_c$, of Eq. (17) in the bulk plasma region (not the sheath) and by the resistive sheath result, $\tilde{K}_{\mathrm{sheath}}$, of Eq. (24) inside the sheath region. In the sheath module, the sheath thickness, Δ, near a solid surface is determined locally by Eq. (26), and the sheath region extends a distance, Δ, normal from the solid surface. The iteration procedure is started assuming a uniform rf power deposition profile in Eq. (4) and a uniform guess for the sheath thickness to calculate the plasma density distribution from the transport module. The electromagnetic module then uses this plasma density distribution to calculate the rf fields and power deposition required to update Eq. (26) for Δ, Eq. (24) for $\tilde{K}_{\mathrm{sheath}}$, and Eq. (4) for $\mathcal{S}$. Relaxation techniques and subiteration are used to stabilize the density profile and the sheath-transport boundary between iterations with the electromagnetic module. A specified fixed uniform neutral density profile and fixed cross sections are assumed for all iterations.

Precise details of the prototype reactor and its results are proprietary, but the normalized measured etch rate profiles for a process that can reasonably be compared with an argon simulation are shown in Fig. 5. For this work, 300 mm Si wafers, coated with 0.5 μm deep ultraviolet (DUV) photoresist, were etched by a very high frequency capacitively coupled plasma with a small amount of conventional 13.56 MHz wafer biasing for several different coil currents in the magnet. Ammonia gas was fed as the main etching gas to suppress excessive chemical reactions that complicate the

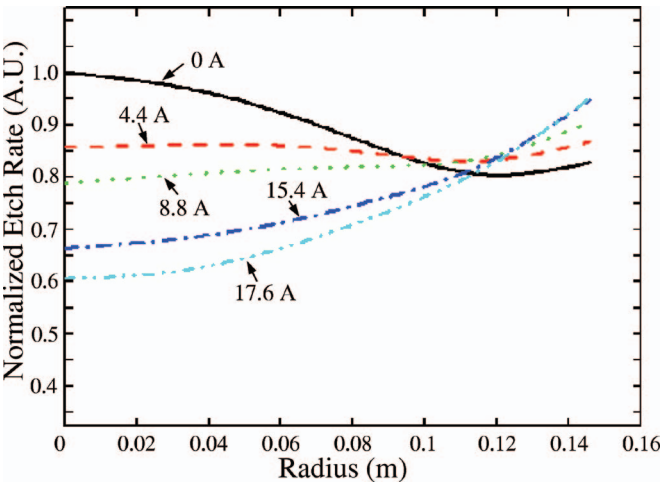

FIG. 5. (Color) The measured radial etch rate profile of 300 mm photoresist blanket wafer etched by NH_3 with a small amount of O_2 in a capacitively coupled plasma with various magnet coil currents at 50 mT operating pressure. Increasing the magnetic field causes the radial etch profile to become hollow.

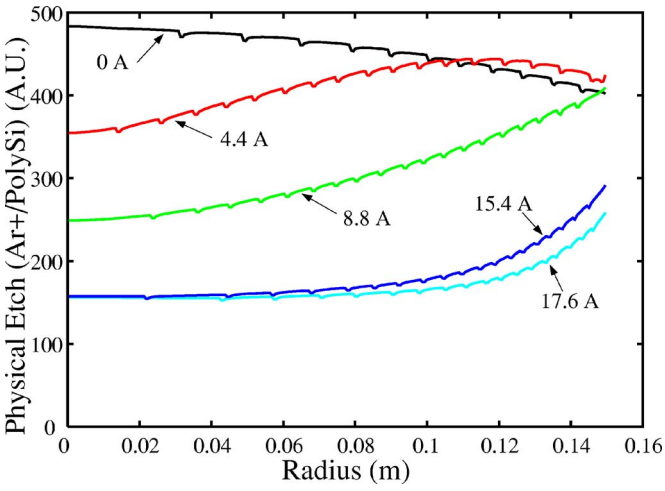

FIG. 6. (Color online) The radial profile of physical etching by Ar in the model of the mockup can be strongly affected by the applied magnetic field, driving the profile hollow near the center of the wafer. $E_{\mathrm{EDF}}=T_e=1.4$ eV, $T_i=0.07$ eV, $n_n=4.6\times10^{20}$ m^{-3}, $\sigma_{et}=5\times10^{-19}$ m^2, and $\sigma_{rlx}=1\times10^{-20}$ m^2.

calculation of the radial etch rate profile in the model, although a small amount of oxygen gas was also fed to avoid etch stop on the resist blanket of the wafer. The data shown were taken for a gas mixture that can reasonably be compared with an argon model of the plasma. The maximum level of very high frequency power was applied to the top electrode in order to keep the source of plasma dominated by power from the top electrode. A small bias power was applied to the bottom electrode to simultaneously maintain the necessary sheath voltage and thickness. At these conditions, the rf voltage measured at the bottom electrode through a *V-I* probe varied between 270 and 290 V depending on coil currents. These results show that a radially peaked profile with no magnetic field can be made flat, or even hollow, by adding a small static magnetic field. This additional control allows the uniformity of the etch or deposition rate to be tuned for more desirable wafer processing independent of other circuit parameters or the gas mixture.

The physical etch rate profiles, using Eq. (29) and the results of the 2D MORRFIC argon model of this system, are shown in Fig. 6. These results also show a transition from a radially peaked profile for no magnetic field[18] to a hollow profile as the magnetic field is increased. The transition in the model also occurs for roughly the same magnet coil currents as those shown in Fig. 5. A uniformly hollow etch profile is observed for coil currents greater than 8.8 A in both the model and the experiment. The slight modulation in the results of the model shown in Fig. 6 appear because the numerical grid spacing in the radial direction is significantly longer than the spacing in the axial direction to improve computational performance. When the sheath thickness changes from iteration to iteration, because of interference patterns in rf waves that are reflected along the sheath layer, corner effects near interference points on the grid can give rise to a slight peaking of the rf field. This physical interference pattern, coupled with the grid "peaking", introduces noise in the model for the sheath thickness, and the slight modulations shown. Increasing radial resolution and over-relaxation techniques can further reduce this numerical noise, but require additional computational resources.

The sensitivity of the modeling results to the parameters that are used provides information concerning the physical processes involved. Two parameters in this relatively simple plasma source model control the magnetic field strength required to produce this hollowing effect. These are E_{EDF} and σ_{rlx}, as discussed in Sec. II A. Both control the spatial volume over which power deposited by the rf can cross magnetic field lines. The values used in Fig. 6 were $E_{\mathrm{EDF}}=T_e=1.4$ eV and $\sigma_{rlx}=1\times10^{-20}$ m^2, with $\sigma_{et}/\sigma_{rlx}=50$. Other important parameters for the modeling were $\sigma_{it}=1\times10^{-18}$ m^2, a neutral fill density of $n_n=4.6\times10^{20}$ m^{-3}, $T_i=0.07$ eV, and $E_{\mathrm{ion}}=200$ eV. The value of E_{EDF} can be adjusted in the model to control the magnetic field strength at which the profile begins to flatten. Increasing E_{EDF} to values greater than T_e, such as might be expected for a strongly heated EDF, raises the magnetic field required for the onset of a flattening effect. Adjusting σ_{rlx} controls the extent to which the hollowing occurs, especially for higher values of the magnetic field. These results demonstrate the need to consider 2D cross-field transport and the 2D distribution of absorbed rf power when modeling magnetized discharges.

The most notable difference between the model results and the experiment is the overall reduction in etch rate with increasing magnetic field in the model. This effect in the model is primarily caused by a radially outward shift in the plasma toward the pump region as the current in the coil is increased. The formation of plasma in the larger volume at larger radius, combined with the roughly fixed global number of electron-ion pairs produced (fixed total rf power and E_{ion}), reduces the plasma density near the center of the discharge as the magnetic field increases. In the actual device, plasma is not produced in the pump region of the discharge because of circuit effects beyond the scope of the model and the three-dimensional nature of the pumping region. However, because the pumping region is grounded along with the wafer chuck in the 2D model, an artificial method must be used to simulate the lack of significant plasma formation in

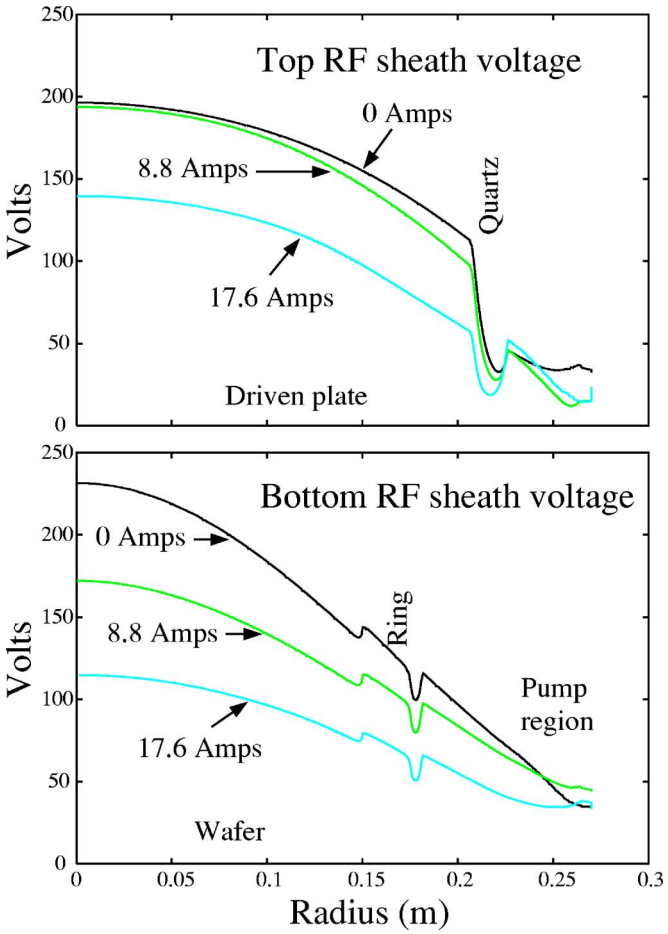

FIG. 7. (Color online) The combined sheath, rf, and transport models produce rf voltages that are not balanced between the top and bottom capacitor plates. The amplitude of the voltages is affected by the static magnetic field, but the peaked shape near the center is not changed.

the pump region, especially for cases with large radial magnetic field components in the pump region. For the modeling results in Fig. 6, the plasma source was artificially set to zero for radii larger than 0.23 m to simulate the lack of production in the pump region, and plasma was allowed to diffuse into the pump region to prevent numerical difficulties associated with an abrupt transition to vacuum. This setting allowed reasonable comparisons with the experiment and was kept the same for all results presented in this paper to minimize its effect on the conclusions. Additional variations between the model and experiment may arise because of small modifications in the oxygen content and the small amount of wafer biasing used in the experiment at 13.56 MHz, both of which are beyond the scope of the model presented here.

Figure 7 shows the rf sheath voltages, V_1, on the top (driven) and bottom (grounded) plates for several different coil currents in the magnet. Note that the top and bottom rf sheath voltages are not symmetric, so the average of the top and bottom values of V_0 from Eq. (28) were used to estimate the etch rate. These profiles flatten somewhat with increasing magnetic field strength, but remain peaked for all of the cases considered here. The sudden transitions in voltage occur when the surface beneath the sheath is dielectric rather than conductor, as labeled (see Fig. 3).

As shown in Fig. 8, the magnetic field primarily affects

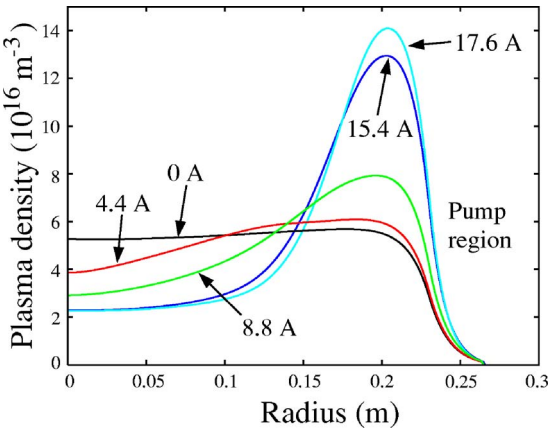

FIG. 8. (Color online) The density halfway between the top and bottom plates gives an indication of the ion flux at the sheaths for different radii for various magnetic fields when the models are iterated to convergence.

the plasma density in the model because of spatial changes in the rf power deposition and confinement of these heated electrons to localize the source. Relatively flat density profiles were found for magnet currents below 4.4 A. For coil currents from 8.8 to 17.6 A, the density was strongly peaked outside the wafer region, although this peaking is influenced by details used to model the pump region.

Figure 9 shows the ionization source from Eq. (4) for each of the converged cases shown in Figs. 6–8. The figure has been vertically stretched to better visualize the plasma in the vertical gap (0.03 m) compared with the full radial extent of the simulation (0.3 m), and reference locations for different radial features have been added for comparison with previous figures. For the neutral parameters considered here, the ionization source is nearly uniform in the case with negligible magnetic field. However, as the magnetic field in-

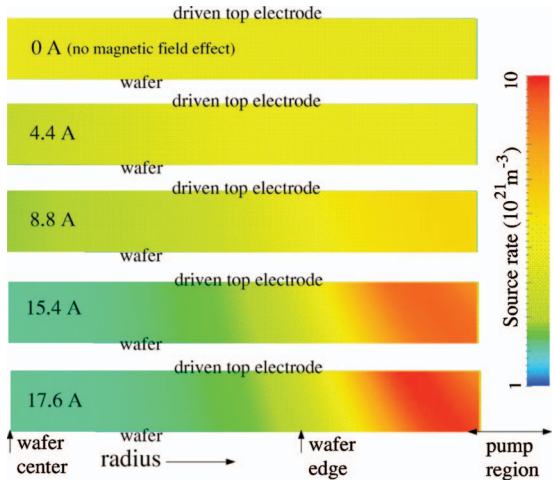

FIG. 9. (Color) The ionization source is affected by the magnetic field because of reduced cross-field heat transport and a redistribution of the rf power toward outer radii with increasing magnetic field for the single coil geometry. As the magnet coil current is increased, the ionizing electrons become more confined by the magnetic field and, at high enough fields, are restricted to move primarily along field lines. This figure has been vertically stretched to better illustrate the effect. For comparison with previous figures, the radial location marked as the wafer edge is at 0.15 m, the thickness of each plasma section is roughly 0.03 m, and the "pump region" begins at a radius of 0.23 m.

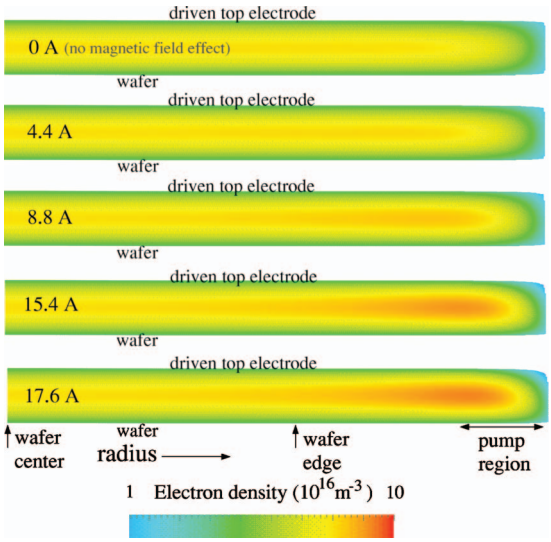

FIG. 10. (Color) Transport modeling results using the same uniform plasma source and all other parameters, except the magnetic field, show only slight enhancement of the plasma density at radii near the wafer edge with increasing magnetic field for a single coil configuration. This figure has been stretched for to better illustrate the effect. For comparison with previous figures, the radial location marked as the wafer edge is at 0.15 m, the thickness of each plasma section is roughly 0.03 m, and the "pump region" begins at a radius of 0.23 m.

creases, the heated electrons are increasingly constrained by the magnetic field. For $E_{EDF}=1.4$ eV, the confinement of the heated electrons becomes important for coil currents as low as 4.4 A, similar to that observed in the experiment. Further increases in the magnetic field lead to increasing density at outer radii which further localizes the rf power deposition at the outer radii.

The effect of the magnetic field on the plasma source can be isolated from the effect of the field on the ambipolar flux by considering a uniform source rate for differing magnetic fields, as shown in Fig. 10. These results were taken from the first iteration of each case in the code such that the source rate and all other parameters are identical, except for the magnetic field strength. Because of the relatively weak effect of the magnetic field on particle transport with uniform power deposition, we conclude that the effects of the magnetic field on the diffusive model of the ambipolar flux are of significantly less consequence than their effect on the ionization source. Again, the gap between plates is 0.03 m and the full radial extent of the simulation is 0.3 m. Reference locations for different radial features have been added for comparison with previous figures.

Through this comparison, we conclude that the rf power deposition primarily determines the plasma source rate, and transport of the plasma along field lines can play a synergistic role in modifying the rf power deposition. The two-dimensional geometry of the system cannot be ignored. These results suggest that the plasma becomes more absorbing because of the increased electron density (rf plasma current) toward the outer radii with increasing magnetic field, and this effect feeds back on itself to move the plasma density distribution outward with increasing magnetic field. However, these results do not completely resolve the question of whether the magnetic field also modifies wave propagation because of the magnetized rf dielectric tensor. Although these studies were performed for rf's above the electron cyclotron frequency at all locations in a highly collisonal plasma, and no cavitylike behavior was observed, which might be expected in the presense of an extraordinary waves or other short wavelength modes, it is possible that the wavelength of magnetized plasma waves could approach the size of the system when the electron cyclotron frequency approaches the driven frequency. Such wave propagation effects could further complicate the synergy. For these plasma parameters, the role of the electrostatic electron Bernstein mode should also be investigated, but this kinetic mode cannot be described by the cold plasma dielectric tensor used in this model.[19]

V. MAGNETIC FIELD COMPONENT EFFECTS

To better understand the physics behind the magnetic field effects on uniformity, it is important to determine the sensitivity of the process to changes in the direction of the magnetic field lines. To isolate the importance of the different magnetic field components, an experiment was performed using a second proprietary tool similar to the one pictured in Figs. 2 and 3, except that a second magnet coil was placed an equal distance below the wafer. Such a coil was also added to the MORRFIC model shown in Fig. 2 with no other changes.

The symmetric magnet coils were operated in three different configurations. The first configuration used only the top coil with varying current increments, similar to the results already presented. The second configuration used currents in the same direction for each coil to form a mirror configuration that eliminates all radial (tangential to the wafer) magnetic field components at the wafer surface. The third configuration used coil currents in opposite directions to form a cusp configuration that eliminates all axial (normal to the wafer) magnetic field components at the wafer surface. For the mirror and cusp configurations, half the current per coil was used relative to the top-coil-only experiments to make the strength of the axial and radial magnetic field components comparable with the top-coil-only cases.

Probe measurements of the plasma density in the experiment with no field, and with the three different field configurations using 5 A of equivalent current, are shown in Fig. 11. These results show that the magnetic field for the cusp configuration has a minimal effect on the radial density profile, while the mirror and top-coil-only configurations show a much stronger, and very similar, dependence on the magnetic field strength. Thus, the axial (normal to the wafer) magnetic field component plays an important role in modifying the experimental etch rate profile.

Results from the model comparing the calculated plasma density halfway between the plates with 4.4 A in the top-coil-only configuration and 2.2 ± 2.2 A for the mirror and cusp configurations, respectively, are shown in Fig. 12. Other parameters in the model are identical with those used in Sec. IV. The effect of magnetic field in the model is very similar to that observed in the experiment, showing only a small effect on the overall transport caused by the cusp fields, but

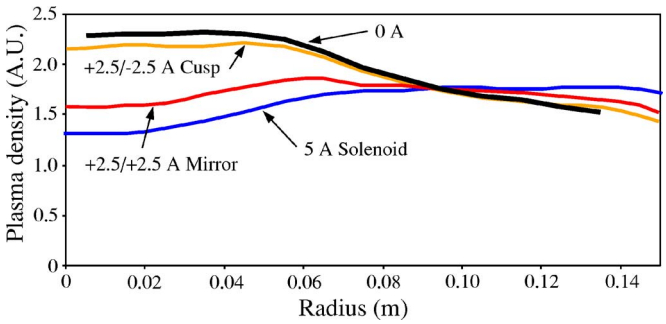

FIG. 11. (Color online) The direction of the magnetic field was changed in the experiment using cusp and mirror configurations. The cusp produces primarily a radial magnetic field throughout the plasma while the mirror produced an axial magnetic field with comparable field strengths. The results indicate that the axial component of the magnetic field plays an important role in controlling the radial density and etch rate profiles.

a much stronger hollowing of the profile with increasing axial magnetic field strength. In the model, the hollowing in the mirror and top-coil-only configurations occurs because of the restricted transport of heated electrons from the outer regions, where the rf power deposition is stronger, to the inner parts of the discharge, where the rf power deposition is weaker. The model also shows a slightly hollow density profile for the case with no magnetic field because of the increased sheath thickness near the center of the discharge (rf voltage peaked at the center). This deviation from the experiment may be partly caused by the methods used to simulate the pump region. But it is also likely an artifact of the diffusive model used for the ambipolar flux and the collisionless approximation used for the sheath.

A more complete, global model of the particle transport, the heat transport, and the sheath processes is needed to accurately model these discharges.[8] However, because similar effects are observed with changing magnetic field in both the model and the experiment, we conclude that the model contains the most basic physical mechanism responsible for the modification of the etch profiles in the experiment. This physical process is a synergy between the magnetic field's effect on the electromagnetic rf power deposition and its reduction of the cross-field transport of rf-heated electrons.

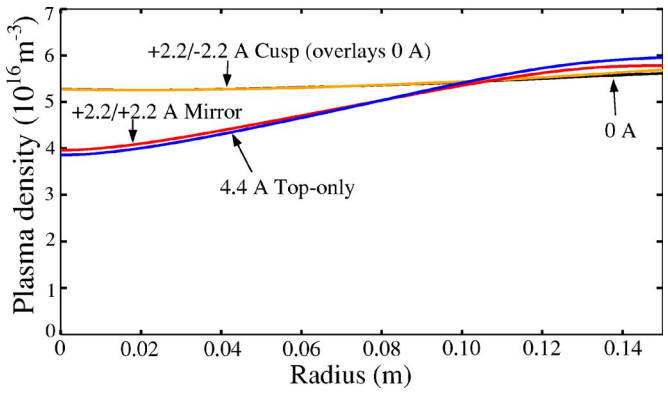

FIG. 12. (Color online) The direction of the magnetic field was changed in the model using cusp and mirror configurations with field component strengths comparable with the top-coil-only case. The cusp produces primarily a radial magnetic field (tangent to the wafer) throughout the plasma, while the mirror produced an axial magnetic field (normal to the wafer) with comparable field strengths. The axial component of the magnetic field plays an important role in controlling the radial density and etch rate profiles by reducing the transport of heated electrons across field lines.

VI. CONCLUSIONS AND FUTURE DIRECTIONS

The effects of a magnetic field on capacitive discharges have been studied using experiments and integrated two-dimensional (2D) physics-based models for rf's above the electron-cyclotron frequency and more than ten times higher than 13.56 MHz. The models were used to survey and identify 2D effects and important physics in relevant devices. A Maxwell solver calculated the electromagnetic rf fields in two dimensions, suitable for very high frequency applications, and the spatial rf power deposition in the magnetized plasma. Analysis of the electron energy relaxation lengths, both along and across magnetic field lines, was used to estimate a spatially varying ionization source rate that was consistent with the deposited rf power and the static magnetic fields. The redistribution of the rf power deposition in space by the transport of heated electrons becomes constrained by the axial magnetic field when $\lambda_\perp = \rho_{\mathrm{EDF}} \sigma_{et} / \sigma_{rlx}$ becomes smaller than the radial scale length for the device ($\lambda_\perp \approx 50 \rho_{\mathrm{EDF}}$ for the conditions considered here), as described in Sec. II A. The rf fields from the Maxwell solver were also used with a collisionless sheath model to create a 2D capacitive layer of finite thickness between solid surfaces and the bulk plasma. A resistive term was added to Maxwell's equations to sustain the ion acceleration within the sheath and consistently extract that power from the electromagnetic fields. A simplified model for the transport of the bulk plasma, using the ionization source and the sheaths, then closed an iterative cycling to convergence between the model's component modules.

The configuration shown in Figs. 2 and 3 was studied with three different magnetic field geometries suitable for qualitative comparison with experimental prototype reactors. In one configuration, a single magnet coil surrounding the system near the top of the device was energized, and etch rate profiles were studied. Two additional configurations used a second coil, located symmetrically below the wafer, to study the effect of the individual components of the magnetic field. For the corresponding experiments, minimal wafer bias was used so that the system was dominated by very high frequency power applied to the top electrode, and the gas composition was chosen to allow reasonable comparison with an argon model. For the model, high frequency rf power was applied to only the top electrode in the model, and the plane of the wafer chuck was treated as a grounded perfect conductor to simulate controlling circuitry in the actual device that was outside the region of simulation.

Experiments from the prototype reactor using a single magnet coil above the plasma showed a transition from centrally peaked to hollow etch rate profiles with increasing magnetic fields. The model was used to estimate the physical etch rate of a pure argon plasma having similar conditions, and good agreement was found with the experiment when appropriate parameters were used. The results indicate that the magnetic field primarily allows a localized increase in the ionization rate for larger radii with increasing magnetic field.

The localization of the plasma source is caused by localized rf power deposition coupled with a reduction in the transport of rf-heated electrons across magnetic field lines with increasing magnetic field strength. The model was also in reasonable agreement with the second experimental reactor having symmetric coils operated in cusp and mirror configurations. These results showed that the static magnetic field component normal to the wafer was primarily responsible for modifying the radial profile of the etch rate, further supporting the finding that the magnetic field reduces the transport of rf-heated electrons across field lines.

In conclusion, we find that a two-dimensional electromagnetic solution is necessary to describe localized rf power deposition in very high frequency systems where the wavelength in plasma becomes comparable with any dimension of the system. The transport of the deposited power and the direction of the magnetic field must be considered, even at very low magnetic field strengths. Although the magnetic field's effect on uniformity was not very sensitive to the diffusive model used for the ambipolar flux, analysis indicates that this diffusive model is not well justified for the devices studied here. Thus, for more detailed modeling, a full solution of the fluid equations may be required in many regimes. The effects of magnetized transport and localized variations in the electron energy distribution should be included if magnetic fields are present. Further improvements in modeling should consider multiple ion and neutral species, collisional sheath models, and possibly effects caused by gas flow. Models for plasmas produced near high power fusion antennas, or in helicons with a high degree of ionization, will certainly require a more detailed self-consistent model of neutral gas distributions.

ACKNOWLEDGMENTS

The authors would like to thank L. A. Berry and E. F. Jaeger of ORNL, and D. A. D'Ippolito and J. R. Myra of Lodestar Research for many useful discussions on the iteration process and rf sheath physics. Oak Ridge National Laboratory is managed by UT-Battelle, LLC, under Contract No. DE-AC05-00OR22725.

[1] M. J. Kushner, J. Appl. Phys. **94**, 1436 (2003).
[2] M. D. Carter *et al.*, Phys. Plasmas **9**, 5097 (2002).
[3] V. A. Godyak, *Soviet Radio Frequency Discharge Research* (Delphic Associates, Falls Church, VA, 1986).
[4] M. A. Lieberman, IEEE Trans. Plasma Sci. **16**, 638 (1988).
[5] A. Fruchtman, G. Makrinich, and J. Ashkenazy, Plasma Sources Sci. Technol. **14**, 152 (2005).
[6] *American Institute of Physics Handbook*, 3rd ed., edited by E. E. Gray (McGraw-Hill, New York, 1972), pp. 8–184.
[7] V. A. Godyak, *1986 Soviet Radio Frequency Discharge Research* (Delphic Associates, Falls Church, VA, 1986); in tenth European Section Conference on the Atomic and Molecular Physics of Ionized Gases, ESCAMPIG90, Orleans, France, 1990, edited by D. Dubreud (unpublished).
[8] V. A. Godyak, N. Sternberg, and D. Hoffman, 32nd IEEE International Conference on Plasma Science, ICOPS 2005, Monterey, CA, June 2005, IEEE (to be published).
[9] G. A. Hebner, J. Appl. Phys. **80**, 2624 (1996).
[10] T. H. Stix, *Waves in Plasmas* (American Institute of Physics, New York, 1992).
[11] E. F. Jaeger, L. A. Berry, J. S. Tolliver, and D. B. Batchelor, Phys. Plasmas **2**, 2597 (1995).
[12] G. Gozadinos, D. Vender, M. M. Turner, and M. A. Lieberman, Plasma Sources Sci. Technol. **10**, 117 (2001).
[13] M. A. Lieberman and V. A. Godyak, IEEE Trans. Plasma Sci. **26**, 955 (1998).
[14] O. A. Popov and V. A. Godyak, J. Appl. Phys. **57**, 53 (1985).
[15] M. A. Lieberman and A. J. Lichtenberg, *Principles of Plasma Discharges and Materials Processing* (Wiley, New York, 1994), p. 354.
[16] V. A. Godyak and N. Sternberg, Phys. Rev. A **42**, 2299 (1990).
[17] J. P. Chang, J. C. Arnold, G. C. H. Zau, H. S. Shin, and H. H. Sawin, J. Vac. Sci. Technol. A **15**, 1853 (1997).
[18] M. A. Lieberman, J. P. Booth, P. Chabert, J. M. Rax, and M. M. Turner, Plasma Sources Sci. Technol. **11**, 283 (2002).
[19] G. Taylor, P. C. Efthimion, B. P. LeBlanc, M. D. Carter, J. B. Caughman, J. B. Wilgen, J. Preinhaelter, R. W. Harvey, and S. A. Sabbagh, Phys. Plasmas **12**, 052511 (2005).

Journal of Applied Physics -- 1 October 2006

J. Appl. Phys. **100**, 073305 (2006) *(13 pages)*

Combined rf and transport effects in magnetized capacitive discharges

M. D. Carter and P. M. Ryan
Oak Ridge National Laboratory, Oak Ridge, Tennessee 37831-6169

D. Hoffman, W. S. Lee, and D. Buchberger
Applied Materials, San Jose, California 94086

V. Godyak
OSRAM Sylvania, Beverly, Massachusetts 01915

(Received 23 January 2006; accepted 12 July 2006; published online 12 October 2006)

Magnetic fields can be used to enhance the performance and operational envelope of rf capacitive discharges for semiconductor processing. Antennas in magnetized experimental fusion devices can experience similar rf processes that lead to surface erosion and degraded antenna performance. Two-dimensional modeling is needed to understand the combined effects of production and transport in these plasmas; however, magnetized plasma is a complicated medium because of tensor rf conductivity, anisotropic transport, and the fact that rf power alone sustains the plasma. In this paper, we give results from a model originally derived for studies of magnetized fusion and helicon discharges that has been adapted to capacitive discharges and compare the results with experimental data. The two-dimensional model combines the effects of the magnetic field on the plasma's rf properties and the bulk transport of plasma, including a sheath layer with finite thickness at the boundaries. A collisionless sheath model uses the rf fields in the sheath region, along with the density at the interface between the bulk plasma and the sheath, to determine the sheath thickness and to estimate the rectified dc potential. The driven rf fields are resolved inside the sheath region by including resistive dissipation caused by ion acceleration. These results are iterated with a model for transport of the bulk plasma to produce a global model of the sheath voltages and bulk rf plasma heating. The results at various iterative steps help isolate magnetic field effects that are caused by modification of the plasma's rf response from transport effects that are caused by the reduced electron mobility perpendicular to the magnetic field. The magnetic field can enhance confinement for some pressure regimes and magnetic configurations. More importantly, the magnetic field can restrict the motion of electrons that are heated by the rf, localizing the nonequilibrium distribution of electron energy and reducing the electron transport across magnetic field lines. Changes in the plasma rf response can also play a role in the behavior of the discharge by further localizing the rf power deposition in the plasma. ©2006 *American Institute of Physics*

doi:10.1063/1.2355436

PACS: 52.80.Pi, 52.25.Fi, 52.40.Fd, 52.40.Hf, 52.40.Kh, 52.50.Qt Additional Information

View ISI's Web of Science data for this article: [Source Abstract | Related Articles]

Full Text: [HTML Sectioned HTML PDF (1177 kB)] Order

References | **All References** | **Scitation Citing Articles** | **CrossRef Citing Articles** | **All Citing Articles**

Only references to articles in journals published by the American Institute of Physics and the American Physical Society are displayed. The complete list of references is available to subscribers only; however, non subscribers have the option to purchase the articles on the below list. For information on reference linking in this journal, click here.

- M. J. Kushner, J. Appl. Phys. **94**, 1436 (2003).
- M. D. Carter et al., Phys. Plasmas **9**, 5097 (2002).
- G. A. Hebner, J. Appl. Phys. **80**, 2624 (1996).
- E. F. Jaeger, L. A. Berry, J. S. Tolliver, and D. B. Batchelor, Phys. Plasmas **2**, 2597 (1995).
- O. A. Popov and V. A. Godyak, J. Appl. Phys. **57**, 53 (1985).
- V. A. Godyak and N. Sternberg, Phys. Rev. A **42**, 2299 (1990).
- G. Taylor, P. C. Efthimion, B. P. LeBlanc, M. D. Carter, J. B. Caughman, J. B. Wilgen, J. Preinhaelter, R. W. Harvey, and S. A. Sabbagh, Phys. Plasmas **12**, 052511 (2005).

Full Text: [HTML Sectioned HTML PDF (1177 kB)] Order

[Previous / Next Abstract | Issue Table of Contents | Top of Page]

[JAP Home] [Browse: All Online Issues] [Search: All Online Issues | SPIN database] [HELP] [EXIT]